Eng. Sci., 2022, **18**, 320–328

Engineered Science

DOI: https://dx.doi.org/10.30919/es8d649

Heavy Metal Removal from Wastewater by a Polypyrrole-derived N-doped Carbon Nanotube Decorated with Fish Scale-like Molybdenum Disulfide Nanosheets

Haitao Zhang,[1,#] Xin Ding,[1,#] Shitao Wang,[1,*] Yan Huang,[1] Xiao-Fei Zeng,[1,*] Srihari Maganti,[2] Qinglong Jiang,[3] Mina Huang,[2, 4] Zhanhu Guo[4] and Dapeng Cao[1,*]

Abstract

Lead (Pb), due to its toxicity, non-biodegradability, and carcinogenicity, has huge harm to the environment and living beings. Therefore, developing an environmentally friendly material to remove lead from wastewater is of extraordinary significance for the health of humans and other creatures. Here, we synthesized a novel N-doped carbon nanotube (derived from polypyrrole precursor) decorated with fish scale-like molybdenum disulfide nanosheet (C-Ppy@MoS_2) by high-temperature hydrothermal reaction and further explored the practical application for removal of Pb(II) from wastewater. Owing to the fish scale-like structure, the C-Ppy@MoS_2 showed a maximum Pb(II) removal capacity of 381.87 mg/g, which is 50 times higher than that of the C-Ppy nanotube without MoS_2 decoration. By one-time filtration removal experiment, it is found that the Pb(II) in the solution after filtration can be almost removed completely, which suggests that the C-Ppy@MoS_2 is an extremely promising adsorbate for the efficient removal of Pb(II) from wastewater.

Keywords: N-doped carbon nanotube; Fish scale-like structure; Removal of Pb((II); MoS_2 nanosheet; Wastewater treatment.
Received: 20 January 2022; 12 February 2022; Accepted: 13 February 2022.
Article type: Research article.

1. Introduction

Currently, heavy metal pollution in water causes serious environmental issues,[1-3] and severely affects human health and living beings.[4-7] For example, Pb(II) is a notorious cumulative neurotoxin. The lead pollution in water is mainly from steel plants, battery factories, and many other industries, and even low concentration levels of lead can cause serious health problems due to its non-degradable property and bioaccumulation.[8-11] Therefore, it is extremely significant for the removal of lead ions from contaminated water.

Various methods have been adopted to remove heavy metal ions from wastewater, including membrane separation,[12,13] ion exchange,[14] chemical precipitation,[15] electrochemical deposition[16], and adsorption technology.[17-24] However, the operating complexity and expensive raw materials greatly limited the application of some techniques in wastewater treatment. The adsorption method shows some advantages for metal ion removal from dilute solutions owing to its high efficiency, design flexibility, and operation convenience,[25,26] and it is therefore regarded as one of the most useful technologies.

Finding a kind of highly efficient adsorbent is urgently required, but still a huge challenge. Nano-adsorbents with many unique physical and chemical properties, like strong operability, high stability, and large specific surface area (SSA), have been developed.[27-34] Further modification of nanomaterials by introducing the sulfur-containing groups can enhance the adsorption and removal ability of heavy metal ions. Moreover, this structure of porous nanosheets can improve the SSA and provide more adsorption sites for the metal ions to increase adsorption performance.[35] Recently, the layered transition metal sulfides attract more and more attention because of the sulfur-functional group.[36-39]

[1] *State Key Laboratory of Organic-Inorganic Composites, Beijing University of Chemical Technology, Beijing 100029, China.*
[2] *Advanced Materials Division, Engineered Multifunctional Composites (EMC) Nanotech LLC, Knoxville, TN 37934, USA.*
[3] *Department of Chemistry and Physics, University of Arkansas, Pine Bluff, Arkansas 71601, USA.*
[4] *Department of Chemical and Biomolecular Engineering, University of Tennessee, Knoxville, TN 37996, USA.*
[#] *Equally contributed to this work.*
**Email:* stwang@buct.edu.cn (S. Wang), zengxf@mail.buct.edn.cn (Zeng), caodp@mail.buct.edu.cn (D. Cao)

Moreover, their low cost, the control of valence states, and high thermal stability make them a promising candidates for metal ion removal.[28,40-44] The investigation from Kong *et al*. indicated that the Pb(II) adsorption amount of iron sulfide (Fe_3S_4)/reduced graphene oxide composites reached 285.71 mg/g.[2] Jawad *et al*. prepared layered double hydroxide (LDH)-based iron-tetrathiomolybdate (Fe-MoS_4) and its Pb(II) adsorption amount was 346 mg/g.[40] Manos *et al*. reported that the Pb(II) adsorption amount of the layered sulfide material $K_{2x}Mn_xSn_{3x}S_6$ reached 329 mg/g.[45] Youngtak *et al*. used porous $Zn_2Sn_xS_{2x+2}$ (x = 1, 2, 4) as an adsorbent and found that its Pb(II) adsorption amount was 331 mg/g.[46] Among transition metal sulfides, the molybdenum sulfide (MoS_2) is an emblematic two- dimensional (2D) material,[47] where each layer consists of one molybdenum sheet sandwiched by two sulfur sheets, forming an S-Mo-S layered structure with six S atoms coordinating with a Mo atom in a trigonal prismatic geometry.[48,49] The MoS_2 is an excellent candidate, due to its special layered structure and forceful combination with heavy metal ions by metal chalcogenides,[50] because S exhibits a strong affinity for soft Lewis acidic metal ions.[51-53] Tong *et al*. synthesized MoS_2/CeO_2 nanohybrids as adsorbents to obtain the capacity of 333 mg/g for Pb(II).[54] Aghagoli *et al*. reported MoS_2-rGO composite and its adsorption capacity reached 322 mg/g for Pb(II).[55] Zhu *et al*. also found that the Pb(II) capacity of MoS_2/ biochar reached 189 mg/g.[56] All these adsorbents with sulfur-functional groups or sulfur edge sites show excellent selectivity for Pb(II) owing to the strong sulfur-lead interaction. Therefore, if the sulfur edge sites can be exposed more efficiently by increasing the SSA of adsorbents, the adsorption amount of adsorbents for Pb(II) would be improved significantly. Based on the fractal concept from mathematics, if the ultra-flaky MoS_2 nanosheets can be used to decorate porous carbon nanotube (CNT), which can significantly increase the SSA of the MoS_2-modified CNT adsorbent and therefore improve its adsorption amount of Pb(II) efficiently.

Here, we use a template method to synthesize the CNTs decorated with fish scale-like MoS_2 nanosheets (marked as C-Ppy@MoS_2) and investigate the performance of the synthesized C-Ppy@MoS_2 sample for Pb(II) removal from wastewater. Then, the effects of different parameters (like adsorption time, adsorbent dose, and metal ion concentration) on the adsorption performance of C-Ppy@MoS_2 are explored systematically.

2. Experimental

2.1 Sample preparation

Figure 1A shows the whole synthesis process using a template method, which is divided into five steps.[57-59] First, we adopted a hydrothermal method to synthesize MoO_3 nanorods (Fig. 1A-1) and further used one-pot oxidative polymerization to synthesize MoO_3@Ppy (Fig. 1A-2) with a core-shell structure. Then, the MoO_3 in the core-shell structure was removed by $NH_3 \cdot H_2O$ (28%) solution to obtain Ppy nanotubes (Fig. 1A-3)[60] and the Ppy nanotubes were subsequently carbonized under an inert atmosphere to obtain N-doped C-Ppy nanotubes (Fig. 1A-4). Finally, the N-doped C-Ppy and $(NH_4)_2MoS_4$ were dispersed in dimethylformamide (DMF), and the filtrated powder was carbonized at high temperature to synthesize C-Ppy@MoS_2 (Fig. 1A-5). Detailed synthesis steps are also presented in Supporting Information.

2.2 Quantitative Pb(II) uptake studies

$Pb(NO_3)_2$ was selected as a representative pollutant for the adsorption study due to its high solubility. The adsorption process was carried out in a fixed shaker. First, the solution with a maximum lead ion concentration of 1000 ppm was prepared using ultra-pure water, and the lower concentration solution could be obtained by subsequent dilution. Batch experiments were performed in 250 mL volumetric flasks under stirring (150 rpm). The effects of different variables, for example, adsorbent dose (5-30 mg), initial concentration (0-110 ppm), and contact time (0-1440 min) on the adsorption performance of Pb(II) were explored. Generally, a certain amount of sample was added to a 250 mL volumetric flask containing 100 mL of heavy metal solution. After the adsorption process was performed for a given period, the mixture was filtered through a nylon membrane filter containing 0.22 μm pores with a medical syringe, and the resulting solution was collected and its Pb(II) concentration was further analyzed by using the inductively coupled plasma-mass spectrometry (ICP-MS) (Agilent Technologies, 7700x (G3281A).

For adsorption kinetics, 10 mg of the as-prepared C-Ppy@MoS_2 was dispersed in a 100 mL solution containing 22.90 ppm Pb(II). The adsorption isotherm was obtained by adding 10 mg of C-Ppy@MoS_2 in 100 mL solutions containing different initial Pb(II) concentrations (0-110 ppm). The amount of lead ion adsorption and the removal efficiency was calculated by the following two equations:

$$q_e = \frac{V(C_0 - C_e)}{W} \quad (1)$$

$$Removal(100\%) = \frac{C_0 - C_e}{C_0} \times 100\% \quad (2)$$

where q_e (mg/g) is the adsorption capacity of heavy metal, V (mL) is the volume of solution, C_0 and Ce (mg/L) are the initial and equilibrium concentrations of Pb(II), respectively, and W (mg) is the mass of adsorbents.

3. Results and discussion

3.1 Characterization

The scanning electron microscopy (SEM) and transmission electron microscopy (TEM) images of the products in each step of the synthesis process are shown in Fig. 1B. MoO_3 nanorods exhibit smooth surface and uniform diameter (Figs. 1B(1-1) and 1B(1-2)). After polymerization, the surface of MoO_3 is coated by Ppy and the TEM image shows the formation of the translucent substances around the MoO_3 nanorods, *i.e.* the formation of the core-shell structure of MoO_3@Ppy (Fig. 1B(2-2)). The hollow tubes can be observed after the ammonia treatment of MoO_3@Ppy (Figs. 1B(3-1)

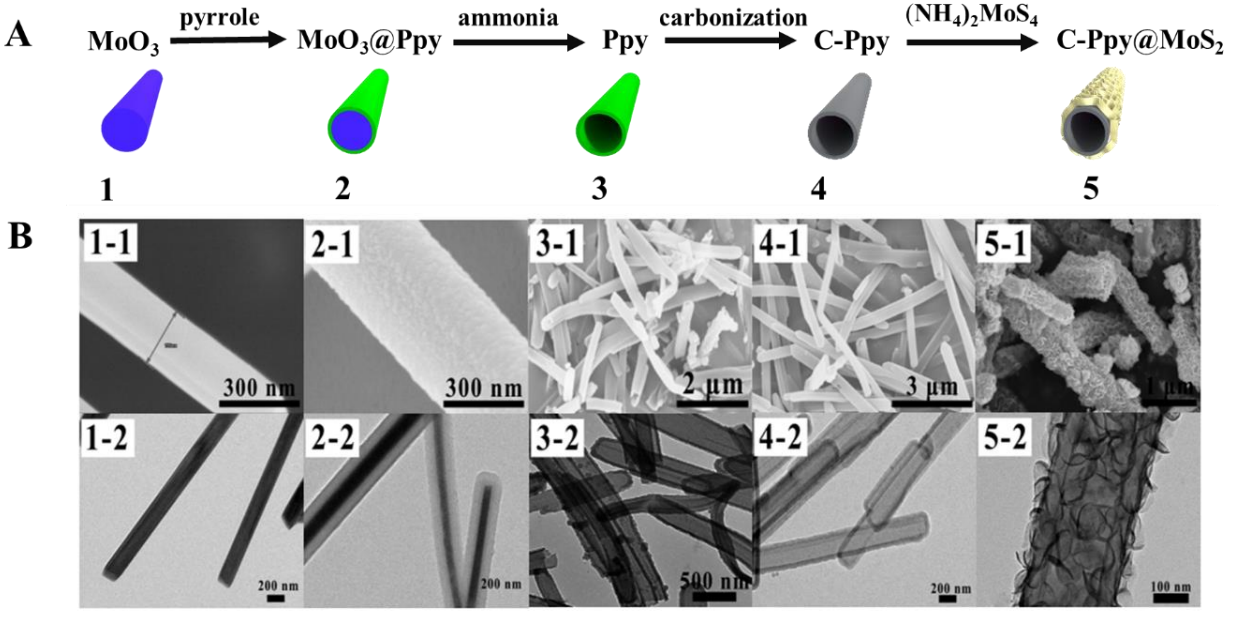

Fig. 1 (A) The synthetic illustration of the C-Ppy@MoS_2, (B) SEM and TEM images of MoO_3 (1-1, 1-2), MoO_3@PPy (2-1, 2-2), PPy (3-1, 3-2), C-Ppy (4-1, 4-2), C-Ppy@MoS_2 (5-1, 5-2).

and (3-2)), and the tubes become more transparent and the tube wall becomes thinner after carbonization (Figs. 1B(4-1) and (4-2)). After the C-Ppy@MoS_2 nanotube was synthesized, the fish scale-like MoS_2 nanosheets are evenly distributed on the surface of C-Ppy nanotubes (Figs. 1B(5-1) and 1B(5-2)).

The X-ray diffraction (XRD) characterization was used to explore the crystal form of materials. As shown in Fig. 2a, all the identifiable sharp diffraction peaks prove the formation of the MoO_3 nanorod crystals. After the pyrrole was polymerized on the surface of MoO_3, the peak position and sharpness are almost the same, indicating that the pyrrole polymerization does not destroy the crystal structure of MoO_3 nanorods. After the MoO_3 nanorods are removed, the sharp peak disappears and only the characteristic peak of Ppy exists (Fig. 2b). After Ppy was carbonized, the degree of graphitization of C-Ppy was characterized by Raman spectrum (Fig. 2c), where the peak ratio of G-band (1560.6 cm^{-1}) associated with graphite crystallinity and D-band (1361.2 cm^{-1}) associated with carbon defects is equal to 1.103, indicating that the material is highly graphitized.

Figure 2d shows that the C-Ppy@MoS_2 sample possesses obvious diffraction peaks of MoS_2 (JCPDS # 75-1539). The peak in the small-angle region, with a d spacing of 0.49 nm indexed to (002) reflections,[53,54] confirms the formation of the MoS_2 nanosheet. In addition, the peaks attributed to the (100) and (110) planes of 2H-MoS_2 in the high-angle region can be found obviously, and the (103) plane could be readily indexed as hexagonal MoS_2. By comparing Raman spectra of C-Ppy (Fig. 2c) and C-Ppy@MoS_2 (Fig. 2e), it is found that an apparent characteristic peak of MoS_2 appears in Fig. 2e.

Raman characterization is also used to investigate the number of layers of each piece of C-Ppy@MoS_2.[61,62] A more detailed structure of the MoS_2 peak in high resolution is shown in Fig. 2f. Based on the Raman mode (ΔK) difference between the in-plane E_{2g}^1 and the out-plane A_{1g}, where the E_{2g}^1 mode is from the opposite vibration of Mo and the two S atoms on either side, and the opposite vibration of the S atom in the opposite direction leads to the occurrence of the A_{1g} mode. Therefore, the layer number of the material can be determined basically. With the increase of the layer number, the E_{2g}^1 the mode shows a red shift while the A_{1g} the mode has a blue shift. The peak frequency difference for bulk MoS_2 is 26 cm^{-1} approximately while it is 24 cm^{-1} for C-Ppy@MoS_2, indicating that the C-Ppy@MoS_2 comprises 3-5 layers of MoS_2.[63] The fish scale-like MoS_2 nanosheets exhibit a layered structure, which significantly increases the SSA of the C-Ppy nanotube and provides more exposed sites for lead adsorption.

Figure 2g clearly shows two peaks of Mo and S elements, suggesting its tubular distribution. The span of elemental distribution is about 200 nm, which is consistent with the tubular size from TEM images. The results further confirm that the sample is a C-Ppy nanotube decorated with fish scale-like MoS_2 nanosheets. The N_2 isotherms of C-Ppy@MoS_2 at 77 K were measured. The BET SSA C-Ppy@MoS_2 reaches 181.95 m^2/g (Fig. 2h), indicating that it contains rich micropores for lead adsorption (Fig. 2i). The detailed parameters are shown in Table S1.

3.2 Batch Pb(II) absorption performance

3.2.1 Effects of adsorbent dose, initial concentration, and adsorption time

Figure 3a shows the effect of the adsorbent dose on the Pb(II) adsorption in C-Ppy@MoS_2. The as-synthesized samples with different doses (5-30 mg) were put into lead nitrate solutions with the same volume (100 mL) of 54.26 ppm. All the adsorption experiments were conducted at T = 25 °C for 24 h.

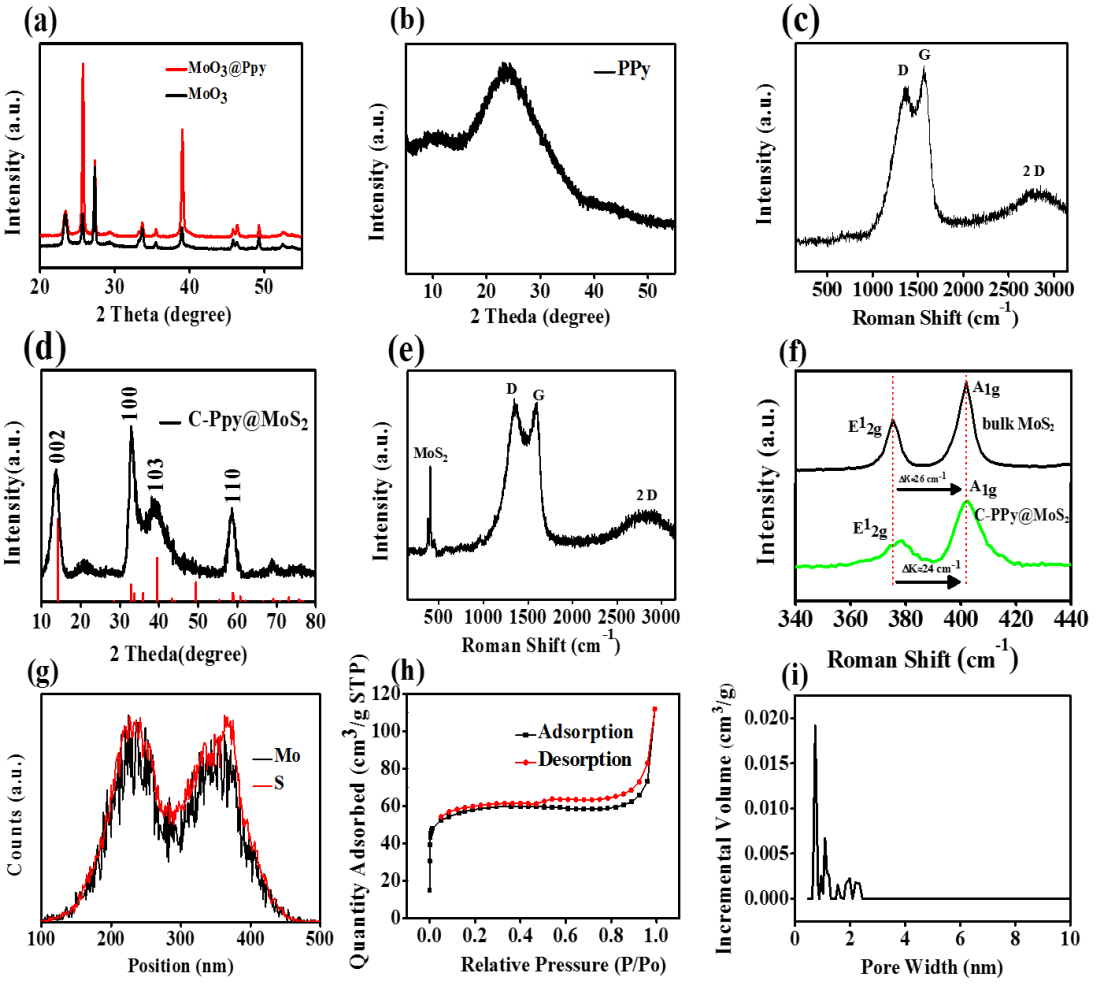

Fig. 2 Structure characterization of as-synthesized samples. (a) (b) XRD pattern of MoO_3, MoO_3@PPy, and Ppy, (c) Raman spectra of C-Ppy, (d) XRD pattern of C-Ppy@MoS_2, (e) Raman spectra of C-Ppy@MoS_2, (f) Magnified Raman spectra of bulk MoS_2 and C-Ppy@MoS_2, (g) Normalized line scan of C-Ppy@MoS_2, (h) N_2 adsorption/desorption isotherms of C-Ppy@MoS_2, (i) Pore size distribution of C-Ppy@MoS_2.

As shown in Fig. 3a, the removal efficiency can reach 82.6% by increasing the adsorbent dose from 5 to 15 mg. When the adsorbent dose is increased to 20 mg, the removal rate reaches almost 100% and does not change anymore. The above results indicate that as long as the adsorbent C-Ppy@MoS_2 is excessive, Pb(II) in wastewater can be removed almost completely.

Adsorption experiments of different concentrations of Pb(II) solutions (0-110 ppm) were performed, where the volume of Pb(II) solutions and the adsorbent doses were fixed at 100 mL and 10 mg, respectively. With the increase of initial Pb(II) concentration (*i.e.* the increase of adsorbate Pb(II) content), the adsorption capacity of Pb(II) in C-Ppy@MoS_2 increases, as shown in Fig. 3b. After the initial Pb(II) concentration increases to 61.04 ppm, the adsorption capacity of C-Ppy@MoS_2 for Pb(II) keeps unchanged, which means that the adsorption capacity of C-Ppy@MoS_2 for Pb(II) reaches it's maximum (here, it is 381.87 $mg \cdot g^{-1}$). When the initial Pb(II) concentration is increased sequentially, the adsorption capacity of Pb(II) in C-Ppy@MoS_2 would be unchanged, i.e. the adsorbates are greatly excessive in this case. Interestingly, as a comparison, the maximum adsorption capacity of Pb(II) in bulk MoS_2 (Fig. S2) and C-Ppy (Fig. 3c) is only about 5~10 $mg \cdot g^{-1}$. The excellent performance of C-Ppy@MoS_2 for Pb(II) adsorption and removal from wastewater is ascribed to the special structure of the fish scale-like MoS_2 nanosheets on the C-Ppy nanotubes.

Figure 3c shows the capacity of Pb(II) at different time intervals, which can reflect the adsorption kinetics of as-synthesized samples. In Fig. 3c, the rapid adsorption efficiency is shown within the first 200 minutes for C-Ppy@MoS_2, and then the adsorption slowly reaches equilibrium, and finally, the removal rate also can reach 100%. The initial adsorption rate is very fast because the adsorbents are greatly excessive and more adsorption sites are available. With the increase of time, the adsorptive sites were occupied gradually. When all the adsorptive sites were occupied entirely, the adsorption capacity of the absorbents would reach the maximum. Figs. 3d-3f show the removal rate and Pb(II) concentration changes with times at three different doses,

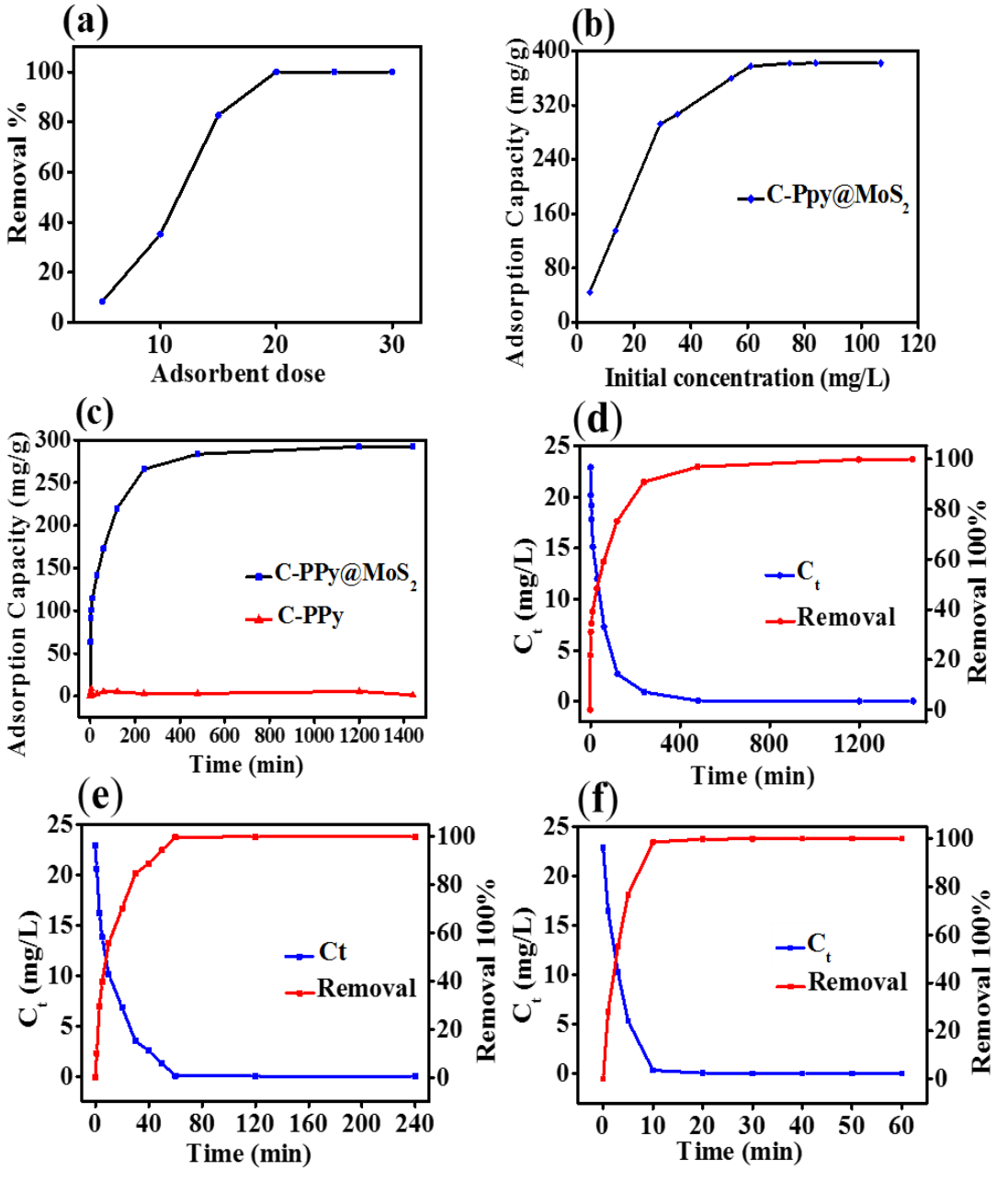

Fig. 3 Adsorption properties of as-synthesized samples. (a) The removal efficiency of Pb(II) by C-Ppy@MoS_2 of different doses, (b) Adsorption capacity of C-Ppy@MoS_2 for Pb(II), (c) Adsorption capacity of Pb(II) in C-Ppy@MoS_2 and C-Ppy changing with time, (d), (e), (f) Removal rate and concentration changes of Pb(II) by different doses of C-Ppy@MoS_2 (10, 30, 50 mg).

where the amount of adsorbents affect the adsorption kinetics. When the amount of adsorbent is 10 mg, it needs about 400 min to reach adsorption equilibrium (Fig. 3d), while when it increases to 30 mg, the adsorption process of Pb(II) will be finished basically in 60 minutes (Fig. 3e). When the adsorbent is increased to 50 mg, the adsorption process only costs about 10 minutes (Fig. 3f). However, the adsorption capacity of C-Ppy for Pb(II) has no significant change with time and concentration, and the adsorption efficiency also has no change (Figs. S3 and 3c). The comparison of C-Ppy and C-Ppy@MoS_2 for Pb(II) adsorption indicates that the presence of MoS_2 indeed affects the adsorption process, where the C-Ppy nanotubes only serve as a support, as expected.

3.2.2 One-time filtration removal experiment

To explore the applicability of C-Ppy@MoS_2,[64] we filtered 50 mL Pb(II) solution with 20 ppm concentration by using C-Ppy@MoS_2-made cake-like material. The operation diagram was shown in Fig. S4. The Pb(II) in the solution after passing the filtration cake (50 mg) can be almost removed completely. The filtration process is about several minutes. This observation indicates that the as-synthesized C-Ppy@MoS_2 sample is an extremely promising adsorbent for the removal of Pb(II) from wastewater.

In addition, we also used Langmuir, Freundlich[65], and Temkin models[66] to investigate the thermodynamics and adsorption mechanism of Pb(II) in the as-synthesized sample

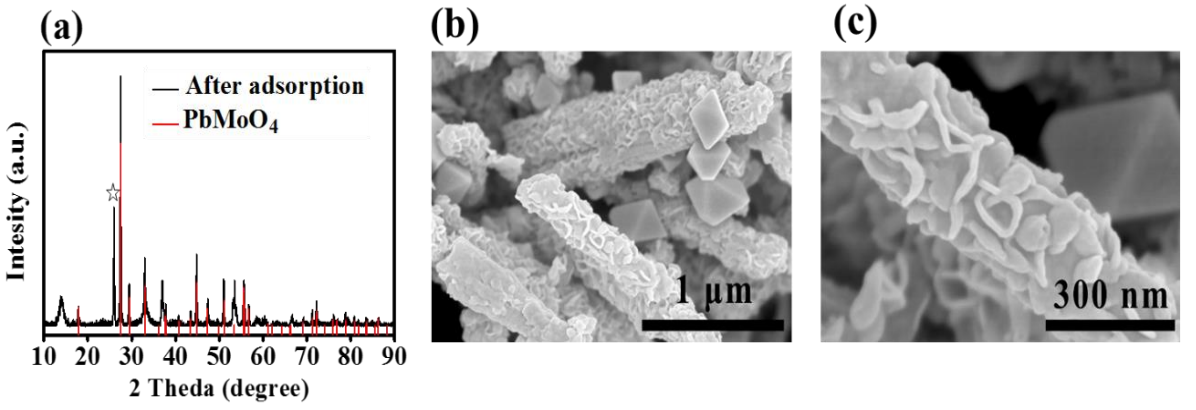

Fig. 4 Characterization of C-Ppy@MoS_2 after adsorption. (a) XRD data and (b, c) SEM images.

(Fig. S5). Results indicate that the Langmuir model can satisfactorily depict the adsorption behavior of Pb(II), which suggests that it is mainly monolayer adsorption. The kinetic equations were also used to explore its adsorption kinetics process.[67] The detailed information is presented in Section S4 in supporting information.

3. 3 Reaction of C-Ppy@MoS_2 with Pb(II)

X-ray diffraction analysis of the sample after adsorption reveals that its XRD is similar to the standard XRD pattern of $PbMoO_4$, as shown in Fig. 4a, where the extra peaks may originate from the presence of other phases. The peak at the position of 28.7° (marked with ☆) indicates that the PbS may be formed due to the strong binding of S to Pb. A single tube for the surface sweep can further prove the substance type of the white block (Fig. S6). The multiple lead energy peaks appear in the corresponding X-ray photoelectron spectroscopy (XPS) spectrum (Fig. S7), and the intensity of S in the XPS may correspond to the inherent selectivity of chalcogenides for Pb(II) ions, where the S atoms replace a part of the O atoms in the $PbMoO_4$. In short, the new type of compound $PbMoO_{4-x}S_x$ may be formed after adsorption.

Figures 4b and 4c show lots of white irregular multifaceted crystals, which can explain the emergence of new substances. At the edge, irregular white crystals were produced, and there were also smaller white blocks in the wall of the tube. The edges of the sheet material are wrinkled, which is similar to the C-Ppy@MoS_2. Therefore, we believe that in the adsorption process, the fish scale-like MoS_2 provided the adsorption sites and most MoS_2 was transferred to $PbMoO_{4-x}S_x$. As a result, the uniform fish scale-like morphology on the surface of nanotubes becomes a gully-like bark structure.

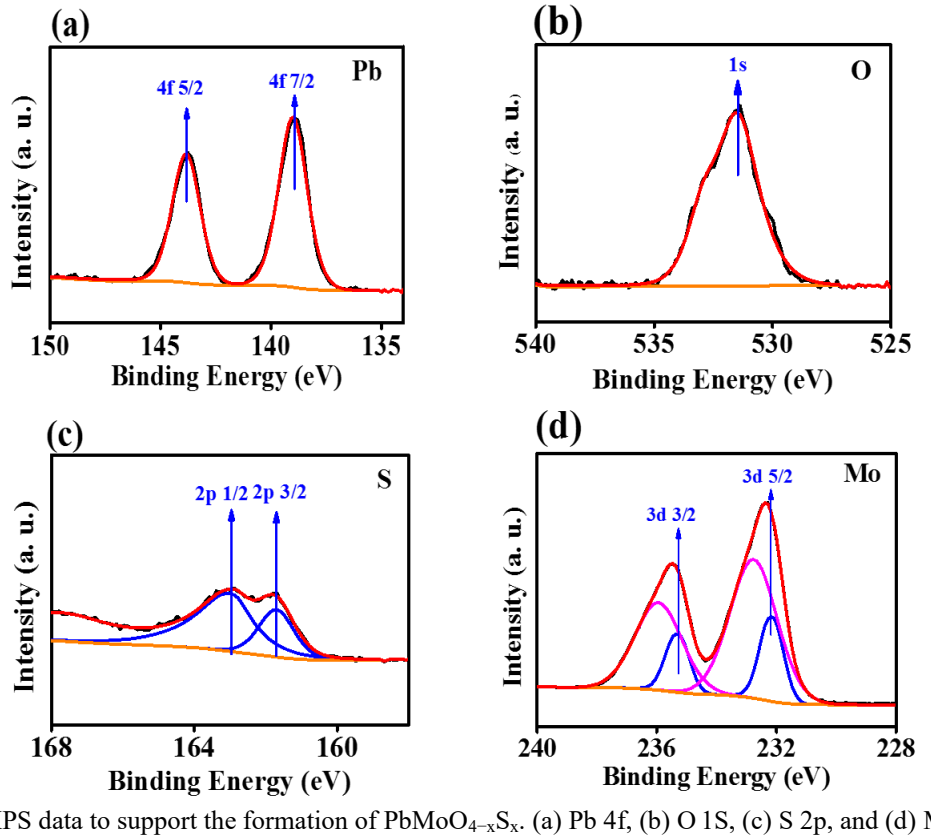

Fig. 5 XPS data to support the formation of $PbMoO_{4-x}S_x$. (a) Pb 4f, (b) O 1S, (c) S 2p, and (d) Mo 3d.

X-ray photoelectron spectroscopy (XPS) was also used to investigate the composition and the states of the elements in the Pb(II)-loaded adsorbents. Fig. S7 shows the full-range scale spectrum of C-Ppy@MoS_2 after adsorption with loading Pb(II). Compared to the binding energies of virgin C-Ppy@MoS_2, an obvious peak about Pb 4f appears. A more detailed structure of the Pb 4f species was obtained in the high-resolution spectrum (Fig. 5a), where the doublet peaks at 143.84 and 138.95 eV indicate that an energy separation of 4.89 eV is attributed to $4f_{7/2}$ and $4f_{5/2}$ of Pb(II) in $PbMoO_{4-x}S_x$. As shown in Fig. 5b, the XPS peak at 531.47 eV agrees with the binding energies of O 1S. In Fig. 5c, the S 2p XPS peaks at 161.71 eV and 162.97 eV are consistent with the binding energies of S $2p_{1/2}$ and S $2p_{3/2}$ related to $PbMoO_{4-x}S_x$. Furthermore, the scan in the Mo 3d region specificity shows two peaks at 235.30 and 232.19 eV, which correspond to the types of oxidation states for MoO_4^{2-} (Fig. 5d). Moreover, it is found that hydrogen gas was generated (from 0 ppmv to 37.2 ppmv) and was detected by a high purity gas analyzer after adsorption test. So, we believe that the protons may have a driving effect on the adsorption process. Based on the above analysis of characterization data, we proposed a possible mechanism[68,69] to present Pb(II) adsorption on the C-Ppy@MoS_2, given by:

$$Mo(IV) + 2H^+ + 4e^- + 4H_2O\ (aq) \rightarrow 5H_2\ (g) + MoO_4^{2-}(VI) \quad (3)$$

$$MoO_4^{2-}(VI) + Pb^{2+} + S \rightarrow PbMoO_{4-x}S_x\ (s) \quad (4)$$

4. Conclusion

In summary, the fish scale-like C-Ppy@MoS_2 was successfully synthesized by the combination of template strategy and hydrothermal method. Owing to the fish scale-like special structure to provide abundant active sites, the C-Ppy@MoS_2 shows excellent performance for Pb(II) removal from wastewater. Results indicate that the C-Ppy@MoS_2 with a fish scale-like structure shows a maximum Pb(II) adsorption capacity of 381.87 mg/g. The material morphology changed significantly after the adsorption of Pb(II) because new crystals were formed due to the innate affinity of chalcogen for Pb(II) ions, and a possible mechanism was also proposed. By one-time filtration removal experiment, it is found that the Pb(II) in the solution after filtration can be almost removed completely. The excellent Pb(II) adsorption performance of as-synthesized materials is attributed to the special structure of the fish scale-like MoS_2 nanosheets on the C-Ppy nanotubes. In short, this work suggests that the fish scale-like C-C-Ppy@MoS_2 is an excellent absorbent for the efficient removal of metal ions from wastewater.

Acknowledgments

This work is supported by the Outstanding Talents Plan from BUCT and Open Fund of State Key Laboratory of Inorganic-Organic Composites, and the Fundamental Research Funds for the Central Universities (buctrc201918).

Conflict of interest

There are no conflicts to declare.

Supporting information

Applicable.

References

[1] Q. Peng, J. Guo, Q. Zhang, J. Xiang, B. Liu, A. Zhou, R. Liu, Y. Tian, *Journal of the American Chemical Society*, 2014, **136**, 4113-4116, doi: 10.1021/ja500506k.

[2] L. Kong, Z. Li, X. Huang, S. Huang, H. Sun, M. Liu, L. Li, *Journal of Materials Chemistry A*, 2017, **5**, 19333-19342, doi: 10.1039/c7ta05389d.

[3] Y. Huang, X. Zeng, L. Guo, J. Lan, L. Zhang, D. Cao, *Separation and Purification Technology*, 2018, **194**, 462-469, doi: 10.1016/j.seppur.2017.11.068.

[4] Y. Li, L. Wang, Y. Wen, B. Ding, G. Sun, T. Ke, J. Chen, J. Yu, *Journal of Materials Chemistry A*, 2015, **3**, 9722-9730, doi: 10.1039/c5ta00608b.

[5] Y. Huang, A. A. Keller, *Water Research*, 2015, **80**, 159-168, doi: 10.1016/j.watres.2015.05.011.

[6] H. Zheng, Y. Gao, K. Zhu, Q. Wang, M. Wakeel, A. Wahid, N. S. Alharbi, C. Chen, *Journal of Colloid and Interface Science*, 2018, **530**, 154-162, doi: 10.1016/j.jcis.2018.06.083.

[7] J. Li, S. Zhang, C. Chen, G. Zhao, X. Yang, J. Li, X. Wang, *ACS Applied Materials & Interfaces*, 2012, **4**, 4991-5000, doi: 10.1021/am301358b.

[8] R. Nevin, *Environmental Research*, 2000, **83**, 1-22, doi: 10.1006/enrs.1999.4045.

[9] S. Wang, J. Hu, J. Li, Y. Dong, *Journal of Hazardous Materials*, 2009, **167**, 44-51, doi: 10.1016/j.jhazmat.2008.12.079.

[10] Q. Liao, J. Tang, H. Wang, W. Yang, L. He, Y. Wang, Z. Yang, *Journal of Hazardous Materials*, 2020, **386**, 121988, doi: 10.1016/j.jhazmat.2019.121988.

[11] S. Zhang, H. Yang, H. Huang, H. Gao, X. Wang, R. Cao, J. Li, X. Xu, X. Wang, *Journal of Materials Chemistry A*, 2017, **5**, 15913-15922, doi: 10.1039/c7ta04377e.

[12] Y. Zhang, S. Zhang, J. Gao, T. S. Chung, *Journal of Membrane Science*, 2016, **515**, 230-237, doi: 10.1016/j.memsci.2016.05.035.

[13] C. Blöcher, J. Dorda, V. Mavrov, H. Chmiel, N. K. Lazaridis, K. A. Matis, *Water Research*, 2003, **37**, 4018-4026, doi: 10.1016/s0043-1354(03)00314-2.

[14] D. Chen, W. Shen, S. Wu, C. Chen, X. Luo, L. Guo, *Nanoscale*, 2016, **8**, 7172-7179, doi: 10.1039/c6nr00695g.

[15] G. Zeng, J. Wan, D. Huang, L. Hu, C. Huang, M. Cheng, W. Xue, X. Gong, R. Wang, D. Jiang, *Journal of Hazardous Materials*, 2017, **339**, 354-367, doi: 10.1016/j.jhazmat.2017.05.038.

[16] Rongzhi Chen, Hisashi Tanaka, Tohru Kawamoto, Miyuki Asai, Chikako Fukushima, Haitao Na, Masato Kurihara, Masayuki Watanabe, Makoto Arisaka, Takuya Nankawa, *Electrochimica Acta*, 2013, **87**, 119-125, doi: 10.1016/j.electacta.2012.08.124.

[17] W. Jiang, Q. Cai, W. Xu, M. Yang, Y. Cai, D. D. Dionysiou,

K. E. O'Shea, *Environmental Science & Technology*, 2014, **48**, 8078-8085, doi: 10.1021/es405804m.
[18] Z. Xiang, Z. Hu, D. Cao, W. Yang, J. Lu, B. Han, W. Wang, *Angewandte Chemie International Edition*, 2011, **50**, 491-494, doi: 10.1002/anie.201004537.
[19] V. Chandra, J. Park, Y. Chun, J. W. Lee, I. C. Hwang, K. S. Kim, *ACS Nano*, 2010, **4**, 3979-3986, doi: 10.1021/nn1008897.
[20] M. Wang, H. Zhang, L. Guo, D. Cao, *Sensors and Actuators B: Chemical*, 2018, **274**, 102-109, doi: 10.1016/j.snb.2018.07.132.
[21] S. Xu, Y. Lv, X. Zeng, D. Cao, *Chemical Engineering Journal*, 2017, **323**, 502-511, doi: 10.1016/j.cej.2017.04.093.
[22] E. Repo, J. K. Warchoł, A. Bhatnagar, A. Mudhoo, M. Sillanpää, *Water Research*, 2013, **47**, 4812-4832, doi: 10.1016/j.watres.2013.06.020.
[23] G. Zhou, J. Luo, C. Liu, L. Chu, J. Crittenden, *Water Research*, 2018, **131**, 246-254, doi: 10.1016/j.watres.2017.12.067.
[24] G. Zhou, J. Luo, C. Liu, L. Chu, J. Ma, Y. Tang, Z. Zeng, S. Luo, *Water Research*, 2016, **89**, 151-160, doi: 10.1016/j.watres.2015.11.053.
[25] J. Zhao, J. Liu, N. Li, W. Wang, J. Nan, Z. Zhao, F. Cui, *Chemical Engineering Journal*, 2016, **304**, 737-746, doi: 10.1016/j.cej.2016.07.003.
[26] M.R. Awual, *Chemical Engineering Journal*, 2015, **266**, 368-375, doi: 10.1016/j.cej.2014.12.094.
[27] K. Xu, W. Li, Q. Liu, B. Li, X. Liu, L. An, Z. Chen, R. Zou, J. Hu, *Journal of Materials Chemistry A*, 2014, **2**, 4795, doi: 10.1039/c3ta14647b.
[28] M. J. Manos, M. G. Kanatzidis, *Chemical Science*, 2016, **7**, 4804-4824, doi: 10.1039/c6sc01039c.
[29] P. Zito, H. J. Shipley, *RSC Advances*, 2015, **5**, 29885-29907, doi: 10.1039/c5ra02714d.
[30] X. Wang, W. Deng, Y. Xie, C. Wang, *Chemical Engineering Journal*, 2013, **228**, 232-242, doi: 10.1016/j.cej.2013.04.104.
[31] W. Tu, Y. Zhou, Z. Zou, *Advanced Functional Materials*, 2013, **23**, 4996-5008, doi: 10.1002/adfm.201203547.
[32] Y. Fu, J. Wang, Q. Liu, H. Zeng, *Carbon*, 2014, **77**, 710-721, doi: 10.1016/j.carbon.2014.05.076.
[33] L. Lv, Y. Huang, D. Cao, *Applied Surface Science*, 2018, **456**, 184-194, doi: 10.1016/j.apsusc.2018.06.116.
[34] Z. Xiang, R. Mercado, J. M. Huck, H. Wang, Z. Guo, W. Wang, D. Cao, M. Haranczyk, B. Smit, *Journal of the American Chemical Society*, 2015, **137**, 13301-13307, doi: 10.1021/jacs.5b06266.
[35] B. Wang, H. Wu, L. Yu, R. Xu, T. T. Lim, X. W. David Lou, *Advanced Materials*, 2012, **24**, 1111-1116, doi: 10.1002/adma.201104599.
[36] X.-Y. Yu, L. Yu, X. W. D. Lou, *Advanced Energy Materials*, 2016, **6**, 1501333, doi: 10.1002/aenm.201501333.
[37] C. Yuan, H. B. Wu, Y. Xie, X. W. D. Lou, *Angewandte Chemie International Edition*, 2014, **53**, 1488-1504, doi: 10.1002/anie.201303971.
[38] S. Wang, B. Y. Guan, L. Yu, X. W. D. Lou, *Advanced Materials*, 2017, **29**, 1702724, doi: 10.1002/adma.201702724.
[39] X. Wang, G. Li, M. H. Seo, F. M. Hassan, M. A. Hoque, Z. Chen, *Advanced Energy Materials*, 2015, **5**, 1501106, doi: 10.1002/aenm.201501106.
[40] A. Jawad, Z. Liao, Z. Zhou, A. Khan, T. Wang, J. Ifthikar, A. Shahzad, Z. Chen, Z. Chen, *ACS Applied Materials & Interfaces*, 2017, **9**, 28451-28463, doi: 10.1021/acsami.7b07208.
[41] D. Sarma, C. D. Malliakas, K. S. Subrahmanyam, S. M. Islam, M. G. Kanatzidis, *Chemical Science*, 2016, **7**, 1121-1132, doi: 10.1039/c5sc03040d.
[42] D. Saha, S. Barakat, S. E. V. Bramer, K. A. Nelson, D. K. Hensley, J. Chen, *ACS Applied Materials & Interfaces*, 2016, **8**, 34132-34142, doi: 10.1021/acsami.6b12190.
[43] L. Ma, S. M. Islam, C. Xiao, J. Zhao, H. Liu, M. Yuan, G. Sun, H. Li, S. Ma, M. G. Kanatzidis, *Journal of the American Chemical Society*, 2017, **139**, 12745-12757, doi: 10.1021/jacs.7b07123.
[44] I. R. Pala, S. L. Brock, *ACS Applied Materials & Interfaces*, 2012, **4**, 2160-2167, doi: 10.1021/am3001538.
[45] M. Manos, M. Kanatzidis, *Chemistry - A European Journal*, 2009, **15**, 4779-4784, doi: 10.1002/chem.200900353.
[46] Y. Oh, S. Bag, C. D. Malliakas, M. G. Kanatzidis, *Chemistry of Materials*, 2011, **23**, 2447-2456, doi: 10.1021/cm2003462.
[47] H. Ramakrishna Matte, A. Gomathi, A. Manna, D. Late, R. Datta, S. Pati, C. Rao, *Angewandte Chemie International Edition*, 2010, **49**, 4059-4062, doi: 10.1002/anie.201000009.
[48] F. Jia, X. Zhang, S. Song, *Physical Chemistry Chemical Physics*, 2017, **19**, 3837-3844, doi: 10.1039/c6cp07302f.
[49] F. Jia, Q. Wang, J. Wu, Y. Li, Shaoxian Song, *ACS Sustainable Chemistry & Engineering*, 2017, **5**, 7419-7419, doi: 10.1021/acssuschemeng.7b01880.
[50] W.Li, D. Chen, F. Xia, J. Z. Y. Tan, J. Son, W. Song, R. A. Caruso, *Chemical communications*, 2016, **52**, 4481-4484, doi: 10.1039/C6CC00577B.
[51] M. L. Feng, D. Sarma, X. H. Qi, K. Z. Du, X. Y. Huang, M. G. Kanatzidis, *Journal of the American Chemical Society*, 2016, **138**, 12578-12585, doi: 10.1021/jacs.6b07351.
[52] M. Wiśniewski, P. A. Gauden, *Adsorption Science & Technology*, 2006, **24**, 389-402, doi: 10.1260/026361706779849744.
[53] W. Kiciński, M. Szala, M. Bystrzejewski, *Carbon*, 2014, **68**, 1-32, doi: 10.1016/j.carbon.2013.11.004.
[54] S. Tong, H. Deng, L. Wang, T. Huang, S. Liu, J. Wang, *Chemical Engineering Journal*, 2018, **335**, 22-31, doi: 10.1016/j.cej.2017.10.056.
[55] M. J. Aghagoli, F. Shemirani, *Microchimica Acta*, 2017, **184**, 237-244, doi: 10.1007/s00604-016-2000-7.
[56] H. Zhu, X. Tan, L. Tan, C. Chen, N. S. Alharbi, T. Hayat, M. Fang, X. Wang, *ACS Applied Nano Materials*, 2018, **1**, 2689-2698, doi: 10.1021/acsanm.8b00388.
[57] M. Zhang, L. Chen, J. Zheng, W. Li, T. Hayat, N. S. Alharbi, W. Gan, J. Xu, *Dalton Transactions*, 2017, **46**, 9172-9179, doi: 10.1039/c7dt01155e.
[58] E. N. Nxumalo, P. J. Letsoalo, L. M. Cele, N. J. Coville, *Journal of Organometallic Chemistry*, 2010, **695**, 2596-2602, doi: 10.1016/j.jorganchem.2010.08.030.
[59] L. Zhao, L. Z. Fan, M. Q. Zhou, H. Guan, S. Qiao, M.

Antonietti, M. M. Titirici, supercapacitors, *Advanced Materials*, 2010, **22**, 5202-5206, doi: 10.1002/adma.201002647.
[60] F. Han, L. Ma, Q. Sun, C. Lei, A. Lu, *Nano Research*, 2014, **7**, 1706-1717, doi: 10.1007/s12274-014-0531-y.
[61] X. Liu, L. Li, Y. Wei, Y. Zheng, Q. Xiao, B. Feng, *The Analyst*, 2015, **140**, 4654-4661, doi: 10.1039/c5an00641d.
[62] C. Tan, X. Qi, X. Huang, J. Yang, B. Zheng, Z. An, R. Chen, J. Wei, B. Z. Tang, W. Huang, H. Zhang, *Advanced Materials*, 2014, **26**, 1735-1739, doi: 10.1002/adma.201304562.
[63] S. Zhuo, Y. Xu, W. Zhao, J. Zhang, B. Zhang, *Angewandte Chemie*, 2013, **125**, 8764-8768, doi: 10.1002/ange.201303480.
[64] K. Ai, C. Ruan, M. Shen, L. Lu, MoS_2Nanosheets with widened interlayer spacing for high-efficiency removal of mercury in aquatic systems, *Advanced Functional Materials*, 2016, **26**, 5542-5549, doi: 10.1002/adfm.201601338.
[65] H. Baseri, S. Tizro, *Process Safety and Environmental Protection*, 2017, **109**, 465-477, doi: 10.1016/j.psep.2017.04.022.
[66] L. Zhang, W. Xia, X. Liu, W. Zhang, *Journal of Materials Chemistry A*, 2015, **3**, 331-340, doi: 10.1039/c4ta05194g.
[67] K. M. Doke, E. M. Khan, *Arabian Journal of Chemistry*, 2017, **10**, S252-S260, doi: 10.1016/j.arabjc.2012.07.031.
[68] L. Tan, Y. Liu, F. Meng, P. Wu, Y. Xia, Y. Tang, *Environmental Science: Nano*, 2020, **7**, 3088-3099, doi: 10.1039/d0en00542h.
[69] N. Kumar, E. Fosso-Kankeu, S. S. Ray, *ACS Applied Materials & Interfaces*, 2019, **11**, 19141-19155, doi: 10.1021/acsami.9b03853.

Author Information

Shitao Wang *obtained B.Sc. degree from Zhengzhou University in 2010 and his M.Sc. degree in 2013 from Shanghai Institute of Organic Chemistry, Chinese Academy of Sciences. He received his Ph.D. degree from The University of Tokyo in 2016 under the supervision of Prof. Makoto Fujita. After a short period of postdoctoral research in the same group, he joined Prof. Virgil Percec's group at the University of Pennsylvania as a postdoctoral researcher (2017-2018), supported by the JSPS research fellowship. Since 2018, he is an associated Professor at Beijing University of Chemical Technology. His current research interests focus on the porous materials and their environment and energy related applications.*

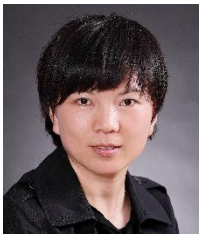

Xiaofei Zeng *is a Professor of the State Key Laboratory of Organic Inorganic Composites at Beijing University of Chemical Technology (BUCT) (2001-). She got her PhD from BUCT in 2010 under the supervision of Professor Jianfeng Chen, and was a visiting scholar at University of New South Wales in Australia (2013-2013). Her research interests are focused on the synthesis of polymer-based energy composites, photoelectric materials and their applications in engineering.*

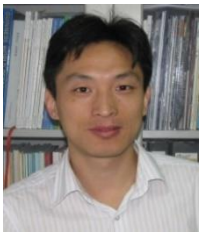

Dapeng Cao *is a Fellow of the Royal Society of Chemistry (FRSC), and a Professor of State Key Laboratory of Organic Inorganic Composites at Beijing University of Chemical Technology (BUCT) (2005-). He received his Ph D degree from BUCT in 2002, and was a research scientist at NanoMaterials Technology Pte. Ltd. in Singapore (2002-2003) and a postdoctoral researcher at the University of California at Riverside (2003-2005). His research interests are focused on the designed synthesis and applications of the porous carbon/organic materials and the energy/catalysis materials.*

